Pressure and shear rate dependence of the viscosity and stress relaxation of polymer melts

Carl Reynolds, Richard Thompson, Tom McLeish

Department of Chemistry, Durham University, Lower Mountjoy, South Road, Durham DH1 3LE

c.d.reynolds@durham.ac.uk

Abstract

The pressure dependencies of polymer viscosity and stress relaxation are an important but often overlooked aspect of the material processing and post-processing properties. We show how these dependencies can be isolated in a single measurement and can be related to the characteristic relaxation times of the material. Using a multi-pass rheometer (a small volume double piston rheometer), a polystyrene melt was confined at 170 °C and pressure range 1-100 bar. The pressure drop over a contraction-expansion geometry and stress birefringence were monitored as a function of shear rate, shear history and applied pressure. Relaxation times, extracted from the stress decays correspond closely to the Rouse and reptation times of the polymer and the contributions of each mode are determined by the relationship between the shear rate and relaxation times established from linear rheology. Increasing the applied pressure caused an increase in viscosity and the measured relaxation time, but no effect on relaxation times was observed with shear rate. The technique allows the extraction of relaxation data following deformation at high shear rates and pressures, conditions more akin to industrial processing than conventional shear rheology.

Introduction

Pressure dependent rheology

While time-temperature superposition principles [1] are routinely used throughout polymer rheology, the pressure dependence of rheological properties is still usually ignored, despite being well known (for example, the reduction in free volume and resulting increase in modulus with increasing pressure is frequently noted [2, 3]). This is in part because it is more challenging to address with standard instruments. For many rheological tests, relaxation times are collected from measurements on open systems such as shear rheometers where it is not feasible to pressurise the sample. However, when these results are then applied to simulations of industrial processes at high pressures (e.g. extrusion, injection moulding), the errors could easily result in using sub-optimal processing conditions. Since the pressure dependence of viscosity was first noted [4], various studies have explored the nature of this dependence in relation to features such as the glass transition temperature [5] and free volume [6]. Pressure dependence of viscosity has generally been found to be greatest for materials that are close to their glass transitions, where it may be expected that a small change in free volume has a large influence on polymer chain dynamics.

One common way of quantitatively expressing the relationship between viscosity and applied pressure is the pressure-viscosity coefficient, which at a given temperature, is defined using the Barus equation [4]:

$$\beta_{T,p} = \frac{d\ ln(\eta)}{d\ p} \tag{1}$$

These values have been recorded for a variety of materials under different conditions, (e.g. PE [7], PMMA [7], PS [7-10]). Most commonly capillary rheometers have been used, usually with an adaptation to regulate the exit pressure [11]. Slit rheometers have also been used for this purpose, for example Volpe *et al.* [9] adapted an injection moulding apparatus to perform

narrow slit experiments, and Kadijk and van der Brule [12] used transducers mounted on the slit wall to remove entry and exit effects.

Sedlacek *et al.* [7] observed that polyethylenes with their regular structure have the least pressure dependence and that adding branching causes pressure to have a greater effect (e.g. β = 10.36 GPa^{-1} for HDPE at 170-210°C but 18.33 GPa^{-1} for LDPE at 150-190°C). Polymers with bulky side groups show greater pressure dependencies (e.g. 43.45 GPa^{-1} for PS at 162-242°C and 43.57 GPa^{-1} for PMMA at 230-250°C). On this basis, it appears that free volume is more significant to the pressure dependence of viscosity rather than other factors such as proximity to a melting transition. A similar trend is well established for the temperature dependence of relaxation time, whereby increasing temperature increases free volume [7, 13, 14].

However, there remains substantial debate on the universality of the β parameter. The pressure-viscosity coefficient has separately been reported to be both dependent and independent on temperature, pressure, shear rate, and results depend on whether shear or extensional viscosity is examined. Other coefficients have been proposed that encompass these dependencies (e.g. on shear rate [15]), but pose extra challenges to verify experimentally. Cardinaels *et al.* [15] have evaluated different methods for calculating the β parameter and concluded that in order to give a true thermodynamic property of the melt, β at constant shear stress was required. The shear rate independent β could still be used, but at high shear rates would include contributions from shear thinning, and hence could be more difficult to interpret. The β value is also seen to vary by measurement technique, which is likely due to the different type of flow generated by different rheometers, for example, a high pressure sliding plate rheometer, which keeps shear rate and pressure uniform [16] was seen to give different values to a capillary rheometer [17], which is less well controlled.

The applicability of a multi-pass rheometer (MPR) for studying rheology under pressure has previously been established [18, 19]. The enclosed system enabled oscillatory rheology to

isolate the elastic and viscous moduli, which is not possible with other process-mimicking techniques such as capillary rheometry [10, 20], and injection moulders [9, 21]. The MPR could also access higher strains than are possible with a rotational rheometer as it does not suffer from sample loss so readily. Although the effects of pressure on steady shear and oscillatory viscosities have been examined previously, early experiments did not have the capability to observe the sample optically and significantly, could not analyse the relaxation of stress.

As well as the change in viscosity, some simulations [22, 23] and dielectric experiments [24] have shown a corresponding increase of the relaxation times of polymers with increasing pressure, and show that the pressure dependence cannot be ignored. This is an important consideration for high pressure processes such as injection moulding, because residual stress in polymers can lead to significant problems of ageing and mechanical weakness in products. In this paper, we use a multi-pass rheometer (MPR4) to provide direct characterisation of viscosity and relaxation as a function of shear rate and shear history. Because the MPR4 can measure pressure difference as well as provide visualisation of stress relaxation, this approach provides a unique opportunity to study this relaxation under pressure. The principle of the MPR in its current form (shown in Figure 1) was first described by Mackley [25], and its use is reviewed in detail by Mackley and Hassel [26]. The salient features for this work are that the MPR allows the extraction

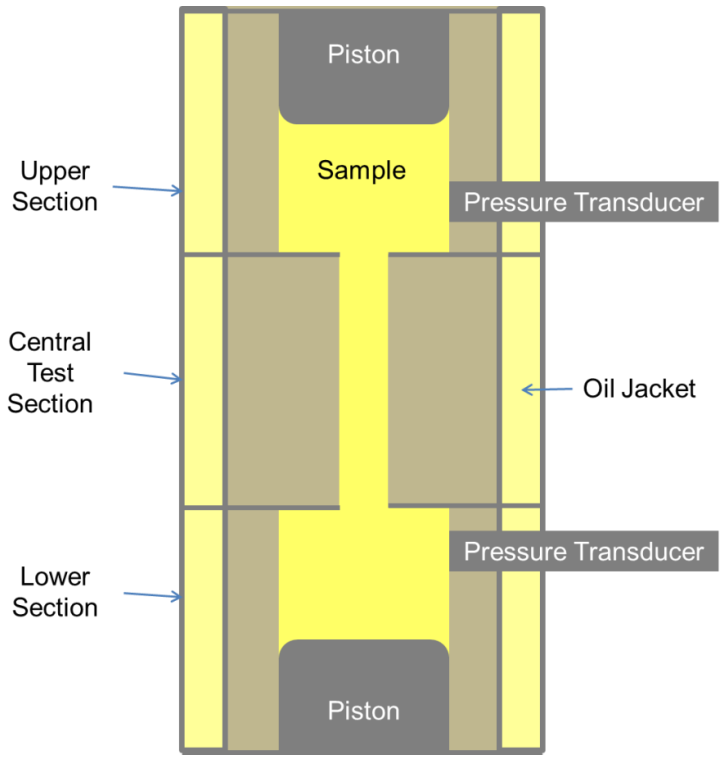

Figure 1: Illustration of the multi-pass rheometer fitted with a narrow slit geometry.

of both simple linear shear data (usually found using a rotational rheometer) and steady shear flow curves (usually found using capillary devices) and obtains both as a function of pressure, as well as pressure-drop, which can be controlled separately in this case [19].

Here, we report the use of a slit geometry with quartz windows at two faces to study stress decay as controlled deformations at high pressures were applied. The resulting decays of both pressure and stress (by examining the decay of stress fringes) are examined as a function of applied pressure and imposed shear rate. Careful analysis of the decay rate enables this to be related to the fundamental relaxation processes of this linear polymer and provides the starting point for predicting pressure dependent relaxation in more complex polymers.

The aim of this work is to provide a detailed interpretation of flow and relaxation under sustained pressure. By combining MPR measurements with size exclusion chromatography (SEC) and rigorous linear rheology of test material, we probe the relationships between pressure, flow, viscosity and relaxation times. This paper is set out as follows: Following the materials and experimental section, we report the linear shear rheology of a PS sample, which is analysed in terms of the molecular weight distribution established by SEC. As well as providing the characteristic reptation and Rouse times of the full molecular weight distribution, this analysis allows these characteristic relaxation times to be calculated for different fractions of the distribution. Results for stress birefringence and pressure drop obtained with the multi-pass rheometer are outlined and analysed to establish the reliability of the method to determine wall shear rates and relaxation times. Derived results for β as a function of flow rate obtained via pressure drop and optical analysis are compared, before we focus on the relaxation times. Stress relaxation cannot be characterised by a single relaxation time, but for most cases is well described by a superposition of two relaxation times; one which is close to the reptation time, and one which is close to the Rouse time, in accord with the standard minimal model emerging from tube theory of polymer melts in nonlinear response [27]. Finally, we show that the polydisperse nature of the polymer used

here (and indeed for virtually all industrial polymers) has significant implications for stress relaxation.

Experimental

Materials

Polystyrene (PS) was supplied by Sigma Aldrich (SKU: 441147). The molecular weight distribution, M_w = 315 kg/mol, M_n = 111 kg/mol, was determined by Gel Permeation Chromatography using a Viscotek TDA 302 with triple detection (Light scattering, viscosity and refractive index) with tetrahydrofuran as solvent at 35 °C and a flow rate of 1 ml/min. The full distribution of molecular weight is given in supplementary material A.

Shear rheometry

To characterise the sample, a disc 1 mm thick with a diameter of 25 mm was pressed in a heated press at 150 °C under 5 tonnes pressure for 5 minutes. Rheological characterisation of this material was performed on a TA AR-2000 rheometer equipped with 25 mm parallel plates and an environmental test chamber under nitrogen gas. Oscillatory frequency sweeps in the range 0.1 rad/s to 600 rad/s were performed at 1 % strain, at temperatures between 130 and 210 ˚C. A Williams-Landel-Ferry (WLF) time-temperature superposition was applied using REPTATE software [28] to overlay the results to produce a single spectrum at a temperature of 170 ˚C.

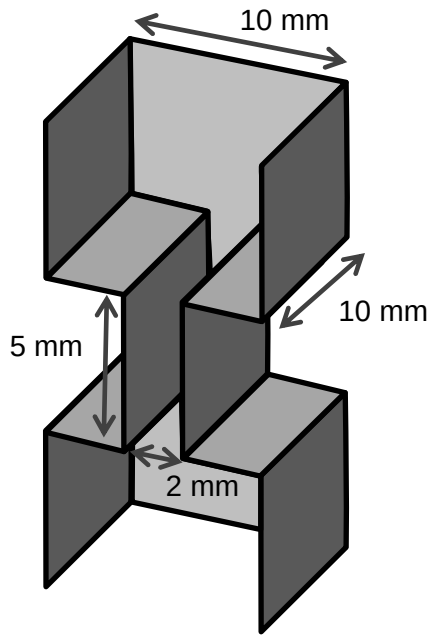

Figure 2: Dimensions of the contraction-expansion geometry.

Multi-pass rheometry

The MPR4 was fitted with a contraction-expansion geometry, with dimensions as given in Figure 2. Approximately 10 g of polystyrene pellets were

loaded into the top and bottom reservoirs and heated to 170 °C with an oil bath connected to jackets around each of the sections, and monitored with three temperature sensors, one in each section. A light source was passed through a 514 nm filter, a linear polariser and a quarter wave plate. The resulting light was used to illuminate the sample through the quartz windows. Video of the sample was recorded during the measurement at 18 fps using a camera fitted with a circular polariser (a combined linear polariser and quarter wave plate) from the quartz window on the opposite side.

The single shot mode of the multi pass rheometer was used in order to reach a steady state and then observe the resulting decay. The pistons were driven towards the geometry to give an initial pressure, before moving both together, one towards and one away from the test section, keeping the spacing constant, in order to create flow through the test section. Pressure transducers in the top and bottom reservoir walls were used to monitor the pressure drop across the geometry. Pressure was recorded at 200 Hz. After allowing sufficient time for a steady state in pressure drop to be reached and the stress fringes to become stable, the flow was stopped. The pressure and stress were continually monitored to observe the decay.

Wall shear rates were calculated using:

$$\gamma = \left(\frac{6Q}{w^2 d}\right)\left(\frac{2+n}{3}\right) \quad (2)$$

where w is the slit width (mm), d the slit depth (mm) and Q is the fixed flow rate (mm^3/s), equal to the piston speed (mm/s) multiplied by the cross-sectional area of the reservoir (π*(reservoir radius (mm))^2). n is the Rabinowich correction factor, determined as 1.59 from the gradient of a log(wall shear rate) vs log(stress) vs graph (plot is included in Supplementary Material A).

Table I: Piston speeds used in these experiments, and the corresponding flow rates in the reservoir, shear rate at the wall and the Rouse and reptation Weissenberg numbers, calculated using τ_D = 3.34 s, the crossover point in the linear rheology, and τ_R = 0.434 s taken from the fit to linear rheology.

Speed (mms^{-1})	Flow Rate (mm^3s^{-1})	Apparent Wall Shear Rate (s^{-1})	Rabinowich Corrected shear rate (s^{-1})	Weissenberg number	
				Rouse	Reptation
0.005	0.39	0.059	0.071	0.031	0.24
0.01	0.79	0.12	0.14	0.061	0.47
0.05	3.9	0.59	0.71	0.31	2.4
0.1	7.9	1.2	1.4	0.61	4.7
0.5	39	5.9	7.1	3.1	24

Experiments were performed at piston speeds between 0.005 mm/s and 0.5 mm/s. The speeds were chosen to span from shear rates that are below both the inverse Rouse and reptation times, to those where both were exceeded (see Table I). For each piston speed, experiments were performed at initial pressures of 1, 3, 10, 30 and 100 bar. It is the initial pressure, applied to the sample before starting the pistons that is used to compare the results. From this point 'pressure' will refer to the pressure initially applied to the sample, and 'pressure drop' will refer to the difference between the values recorded by the two transducers.

Results

Shear rheology

The shear rheology results are shown in Figure 3. A fit was performed using double reptation theory [29-31] using REPTATE [28] software, and is also shown along with the parameters used. The range of molecular weights, obtained using Gel Permeation Chromatography (and shown in supplementary material A), was discretised to 20 values per decade of molecular weight and used as input for the theory. Materials parameters, τ_e (Rouse time of one entanglement segment) G_e (entanglement modulus) and M_e (entanglement molecular weight) were all fitted to the data, and values are included in Figure 3. The molecular weight

of a Rouse monomer, M_0 was kept to a value of 0.001 kg/mol as recommended [32] and α, which is the dilution exponent for treating constraint release, was set to a value of 1.3, in accordance with the recommendation of Van Ruymbeke *et al.* [33]. This gave values for τ_e G_e and M_e that were consistent with established literature values for polystyrene. An estimation of the weight-averaged Rouse time can be given by,

$$\tau_R = \sum^{a} \tau_e \left(\frac{M_{wa}}{M_e}\right)^2 w_a \tag{2}$$

where M_{wa} is the molecular weight and w_a is the weight fraction of that molecular weight from the GPC. This was calculated over the range of molecular weights in the GPC, giving a value of 0.434 s. The reptation time was taken as the inverse of the low frequency crossover in G' and G'', giving a value of 3.34 s.

It is important to note that the variety of polymer molecular weights present in even a moderately polydisperse sample implies that the material contains a mixture of chains possessing a range of Rouse (stretching) and reptation (orientation) times. In order to further

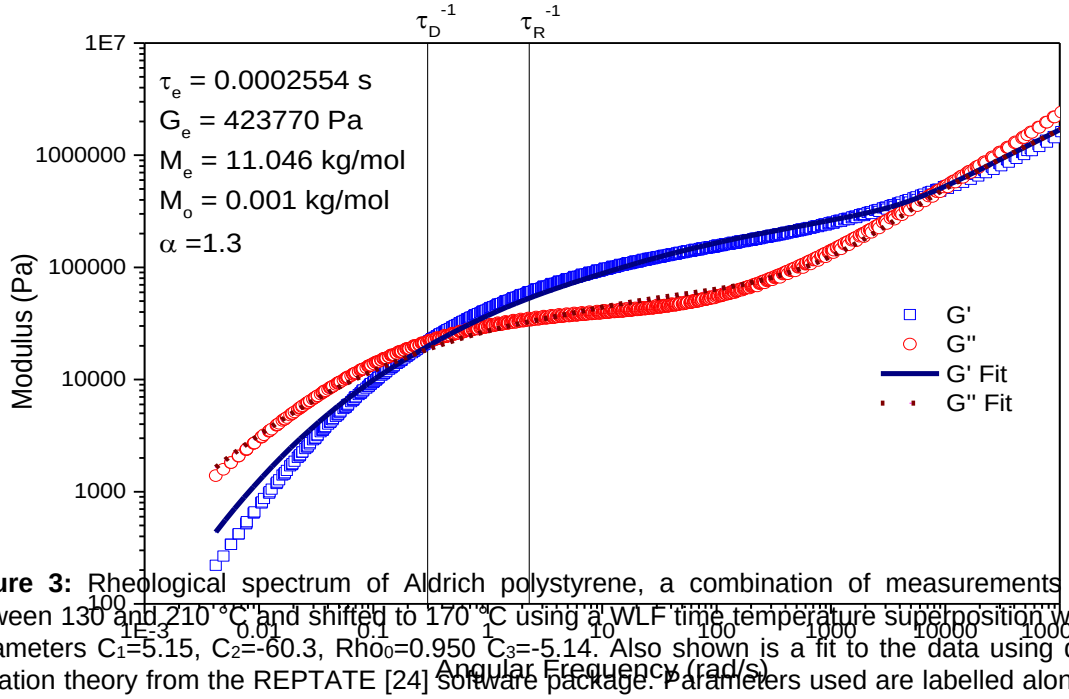

Figure 3: Rheological spectrum of Aldrich polystyrene, a combination of measurements made between 130 and 210 °C and shifted to 170 °C using a WLF time temperature superposition with the parameters C_1=5.15, C_2=-60.3, Rho_0=0.950 C_3=-5.14. Also shown is a fit to the data using double reptation theory from the REPTATE [24] software package. Parameters used are labelled along with the Rouse time (extracted from the theory) and reptation time (crossover in G' and G''). τ_e represents the Rouse time of one entanglement segment, G_e is the entanglement modulus, M_e is the entanglement molecular weight, M_0 the molecular weight of a Rouse monomer and α is the constraint release parameter.

explore the effect of polydispersity, the proportion of chains with Rouse and reptation Weissenberg numbers above 1 was calculated for each shear rate. The REPTATE [28] materials database was used to identify values for the molecular weights of polystyrene at 170 °C required to give a reptation Weissenberg number, Wi_d of 1 at each speed, and the GPC results were used to calculate the weight fraction of chains exceeding this molecular weight For the Rouse times, Equation 2 with the materials parameters from the fits was used to calculate the molecular weight corresponding to a Rouse Weissenberg Wi_R number of one. The results are summarised in Table II.

The linear rheological characterisation was also repeated on a sample after the MPR experiments were performed, to check for degradation, confirming no change, which is expected for polystyrene which is relatively stable with respect to oxidation at 170 ˚C.

Multi-pass rheometry

In order to confirm there was no significant pressure loss over an experiment, the mean pressure (average of values at top and bottom pistons) was monitored throughout each experiment. No significant change in mean pressure was noted on starting the movement of the pistons, although the individual transducers' values changed due to the pressure drop

Table II: Calculated weight fractions of chains above their Rouse and reptation times for each piston speed used, calculated from the GPC results and using the REPTATE [24] materials database.

Speed / mms^{-1}	**Rabinowich Corrected Wall Shear Rate / s^{-1}**	***M* (Wi_d=1) /gmol^{-1}**	**Polymer chain fraction above M (Wi_d=1)**	***M* (Wi_R=1) /gmol^{-1}**	**Polymer chain fraction above M (Wi_R=1)**
0.005	0.071	358000	0.308	2950000	0.000891
0.01	0.14	293000	0.381	2080000	0.00360
0.05	0.71	186000	0.541	933000	0.0503
0.1	1.4	154000	0.607	660000	0.118
0.5	7.1	99600	0.730	295000	0.379

across the geometry, as shown in Figure 4 and observed previously for pre-pressurised MPR experiments by Valette *et al.* [34].

On cessation of movement, some decrease in mean pressure was noted over very long times (~10 % over ~40 minutes at 100 bar). However, the applied deformations were short (< 1 min) and the data analysed from the stress relaxation was within the first 20 s of stopping the pistons, when the mean pressure and the recovered pressures at each piston after the decay, were not significantly different from their initial values. Hence it is valid to assume that the initial pressure applied to the sample was maintained throughout the experiment.

In each experiment, the number of observed fringes was seen to increase as the flow was established until a constant state was reached. Typical results for the build-up of fringes as

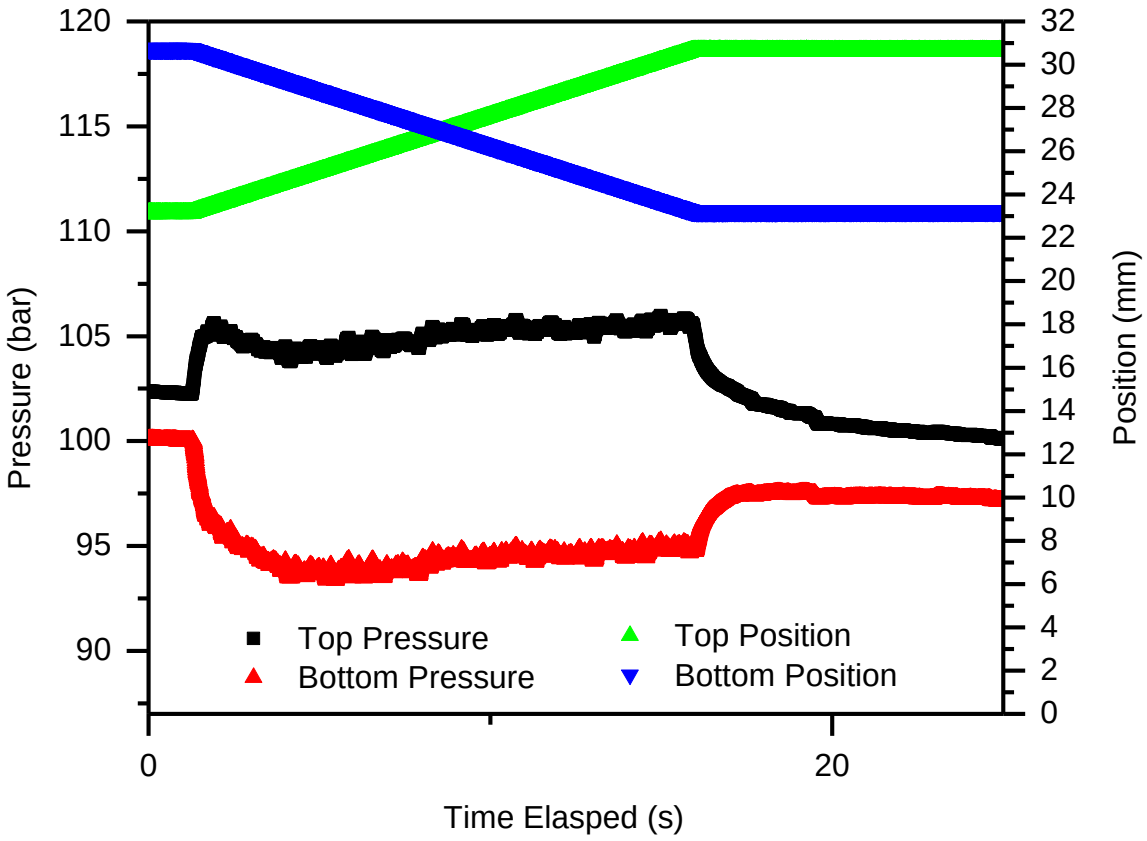

Figure 4: Values of the pressure and position of individual transducers during an experiment at 100 bar initial pressure and a speed of 0.5 mm/s.

flow is established are shown in Figure 5. Once the steady state is established, it is possible to select an individual frame and measure the stress within the geometry by counting the fringes as is shown in Figure 6.

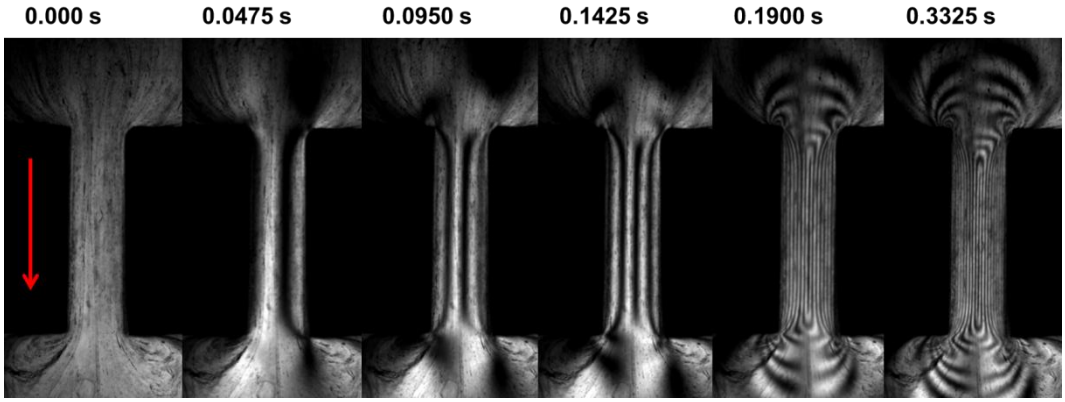

Figure 5: Build-up of stress fringes to a steady state as PS is driven through a narrow slit at a piston speed of 0.5 mm/s under 30 bar of initial pressure at 170 °C. Arrow shows flow direction

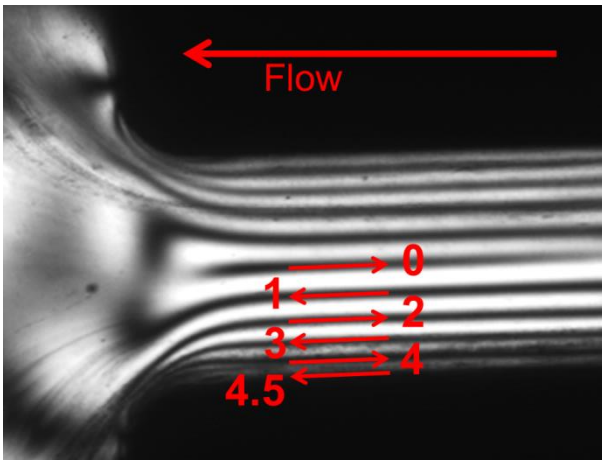

Figure 6: Stress birefringence image of polystyrene flowing through a narrow slit, showing how fringes are counted outwards from the zero fringe, including half a fringe counted for the dark area at the wall.

The difference between the pressure at the top and bottom transducers (the 'pressure drop') was calculated in order to measure the pressure drop across the geometry. The time dependence of pressure drop reveals the steady state condition, where the pistons are moving at constant velocity and the pressure drop is constant (Figure 7). An average value of the pressure in this region was recorded.

The wall shear stress σ_w, was calculated from the steady state pressure drop, in the contraction region of the geometry according to,

$$\sigma_w = \frac{Pressure\ drop\ (Pa) * Flow\ area\ (m^2)}{Wall\ surface\ area\ (m^2)} \quad (3)$$

where the flow area is the cross sectional area of the contraction. The wall shear stress can be related to the number of stress fringes observed via the Stress Optic Coefficient (SOC) which was calculated. This was done for a variety of experiments at different piston speeds and pressures. An average value for the SOC of 4.9 ± 0.2 x 10^{-9} Pa^{-1} was obtained for polystyrene, which was consistent with previously published values [35, 36]. This method is discussed in more detail and the resulting plot shown in the supplementary material B.

Steady state stresses and pressure drops

The wall shear stress was obtained by two methods; firstly the number of fringes at the

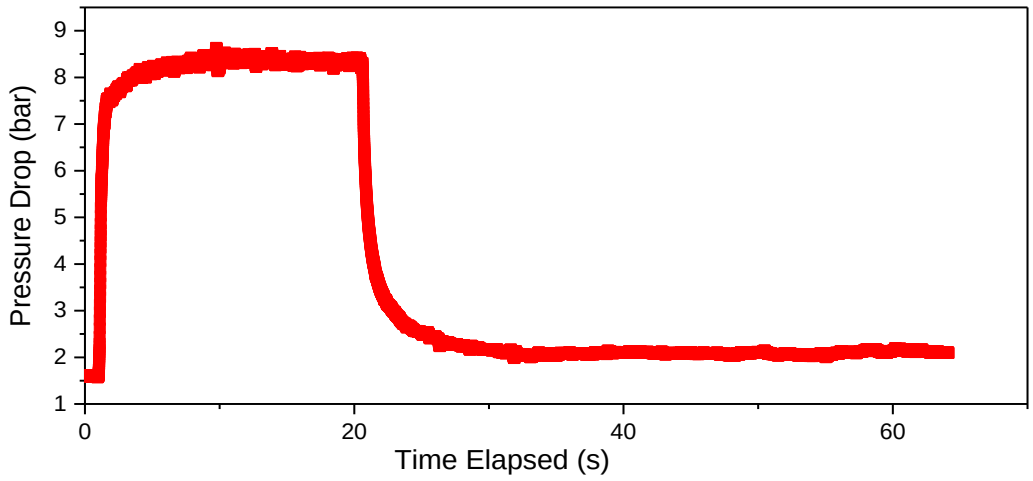

Figure 7: Pressure drop over the contraction-expansion geometry for PS at 0.5 mm/s and 170 °C, with 30 bar of initial pressure, showing the initial build up to a steady state and then decay.

steady state was counted and multiplied by the SOC. Secondly, the pressure drop was measured at steady state and converted into a stress (see calculation of the SOC in supplementary material B for details). The apparent shear viscosity was then calculated by dividing the steady state values of the stress by the wall shear rate. Both these methods are compared to the complex viscosity (measured in the oscillatory test) and steady shear viscosity measured in the rotational rheometer in Figure 8. Values for the pressure dependence of viscosity, β were obtained using Equation 1, and the results are shown in Figure 9. β values were not extracted from the stress fringes for the two slowest speeds, because the change in the number of fringes with pressure was not above the measureable error (0.5 fringes). However these speeds could be analysed by the pressure drop.

Pressure drop decays

An example of the decay in pressure drop over the geometry, after stopping the pistons, is shown in Figure 10. The zero time (when the pistons stopped) was calculated from the starting time and the duration of the deformation. It was noted that the pressure drop did not

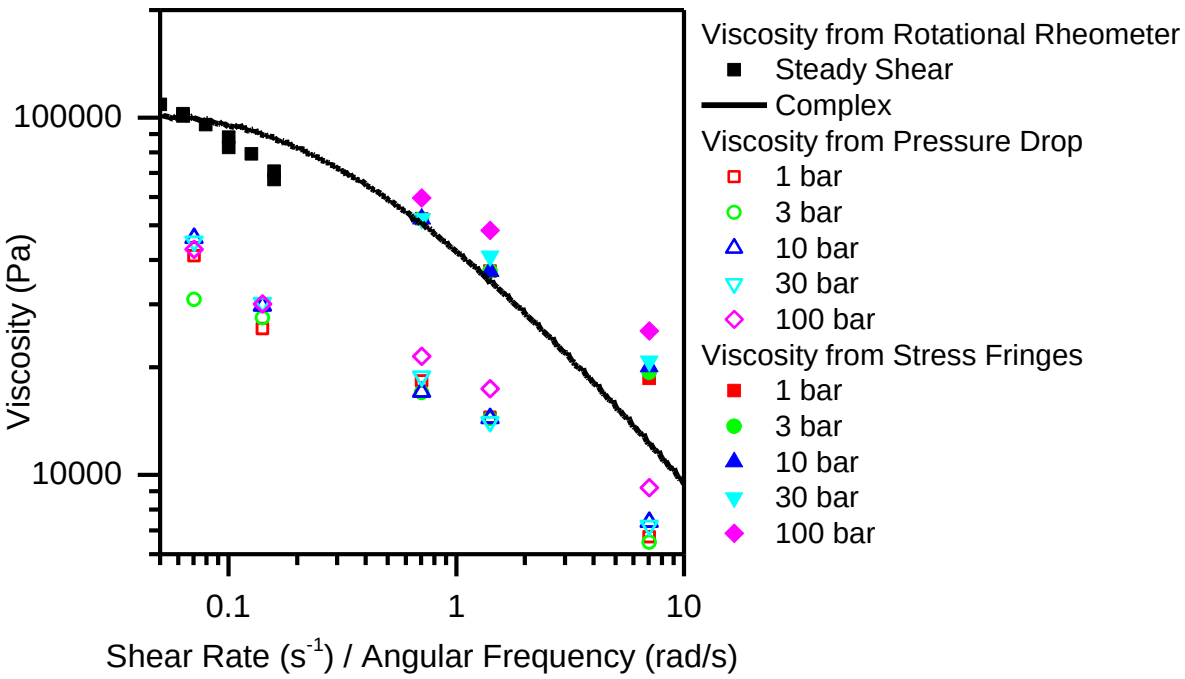

Figure 8: Comparison of the viscosity measured from the fringe count and pressure drop at the steady state with the complex viscosity extracted from oscillatory rheology

return to zero over the window of observation. Because all the stress fringes had decayed at this time, it is valid to assume that this was not due to relaxation in the slit.

The pressure decays could not be represented by a single exponential decay. However, a combination of exponentials with different relaxation times gave good fits. In some decays, as many as three regions were observed, as there was seen an initial fast decay, at short times (usually <0.1 s) in addition to two slower relaxation timescales. Hence the pressure drop decays could be fit with a three term exponential decay, including an offset term, given by:

$$\frac{\Delta P}{\Delta P_0} = \mathrm{y}_0 + A_p exp\left(-\frac{t}{\tau_1}\right) + B_p exp\left(-\frac{t}{\tau_2}\right) + (1 - A_p - B_p) exp\left(-\frac{t}{\tau_f}\right) \quad (4)$$

where ΔP is the pressure drop, ΔP_0 the initial pressure drop, t the time after pistons are stopped, y_0 the fitted offset, τ_1, τ_2 and τ_f are the fitted timescales and A and B are fitted magnitudes of the decays. τ_1 is an early relaxation time which appears to correspond to the Rouse time, τ_2 is a late relaxation time which is consistent with the reptation time and τ_f is included to represent the initial fast decay. The coefficients *A* and *B* therefore represent the relative contributions of the early and late relaxation processes respectively. Although the initial fast decay may not be exponential, it is so brief that it can be approximated by including a single exponential term alongside the early and late relaxations, giving Equation 4.

As most decays were at shear rates slower than the calculated inverse Rouse time, the τ_1 term was not always necessary. τ_1 was noted at the three highest shear rates, where the late relaxation time was observed at all shear rates. Also τ_f was only observed at the highest shear rates. For the lower shear rates, the effect of the initial fast decay was not significant enough to be observed, so the τ_f term could also be excluded. The decays were fitted using the minimum possible number of terms that yielded significantly different relaxation times. The magnitudes of the fast and early relaxation times were similar in all

experiments but the fast relaxation time was always below 0.21 s and could be distinguished from the early relaxation time. All the parameters of the fits and their uncertainties are given in supplementary material C.

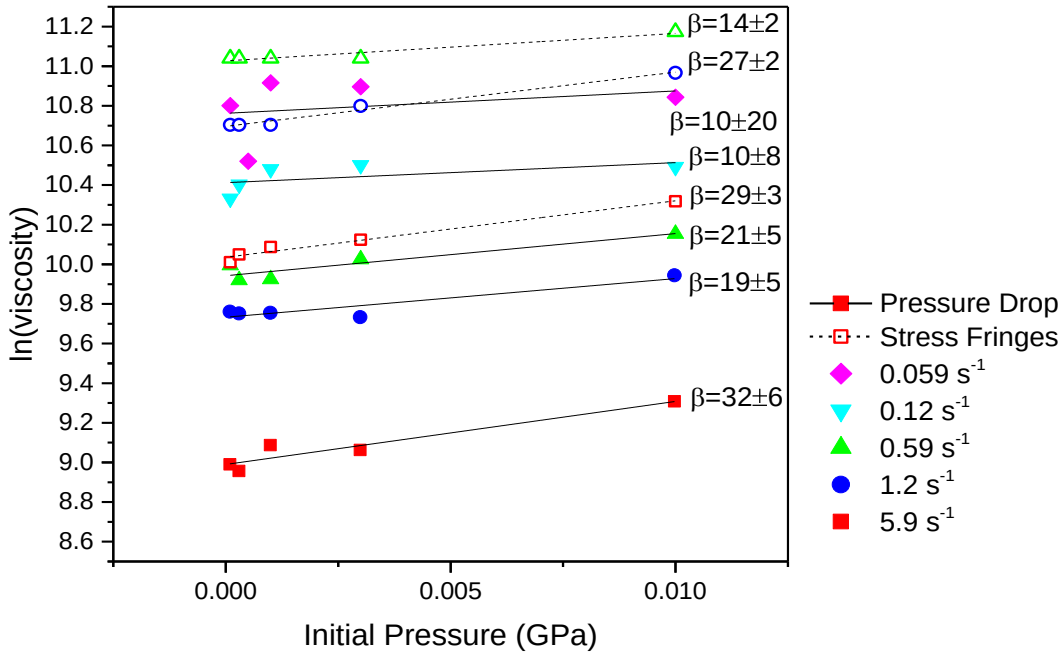

Figure 9: Steady state viscosities measured from pressure drop and stress fringes, labelled with gradients in GPa^{-1}, equal to β in Equation 1. Pressure drop data are represented by solid symbols and solid lines. Stress birefringence data are shown as open symbols and dotted lines. The two slowest shear rates did not create enough stress fringes to capture a change with pressure above the error (0.5 fringes) and hence the viscosities from stress fringes are not included.

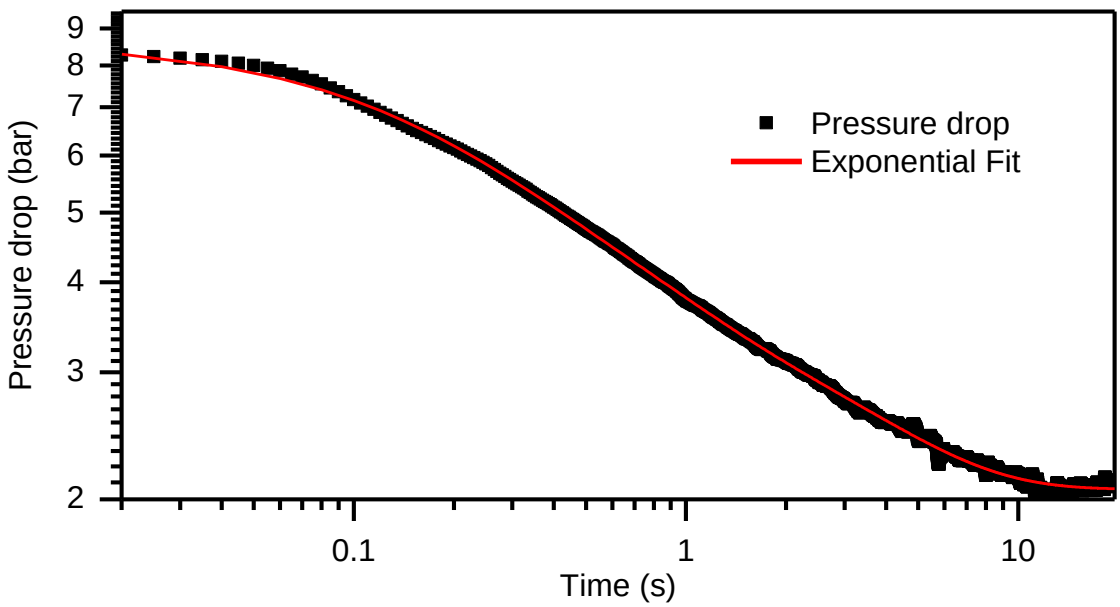

Figure 10: Pressure drop decay of polystyrene after a deformation at 6.9 s^{-1} with 30 bar initial pressure applied. The red curve is the result of a multi-exponential fit using Equation 4.

Stress decays

As the video recording was started independently to the piston movement, the zero point for the decays was instead taken as the point at which the fringes begin to decay. The stress analysis has been focussed on the three highest shear rates because they show sufficient fringes to allow accurate characterisation of the stress decay within the error of counting the fringes. Examples of these decays can be seen in Figure 11.

Multiple exponential decays were again necessary in order to fit the stress relaxation process; the stress decays were fitted to an exponential decay with Equation 5,

$$\frac{\sigma}{\sigma_0} = \mathrm{y}_0 + A_\sigma exp\left(-\frac{t}{\tau_1}\right) + B_\sigma exp\left(-\frac{t}{\tau_2}\right) + (1 - A_\sigma - B_\sigma) exp\left(-\frac{t}{\tau_f}\right) \quad (5)$$

where σ is the stress, σ_0 the initial stress, t the time after pistons are stopped, y_0 the fitted offset, τ_1, τ_2 and τ_f are the fitted timescales and A and B are fitted magnitudes of the decays. Because the stress decayed to zero in every case, the offset term, was constrained to +/- half a fringe (~5000 Pa) to account for any error in fringe counting. This approach gave good fits to the observed stress decays for all of the data (see Figure 11). The early relaxation time, τ_1, was typically of the order of 1 s or less, and was consistently observed at the highest speed, and in some of the decays at lower speeds. The late relaxation τ_2 was observed at all speeds, and was generally found to be in the range 1-4 s. The initial fast

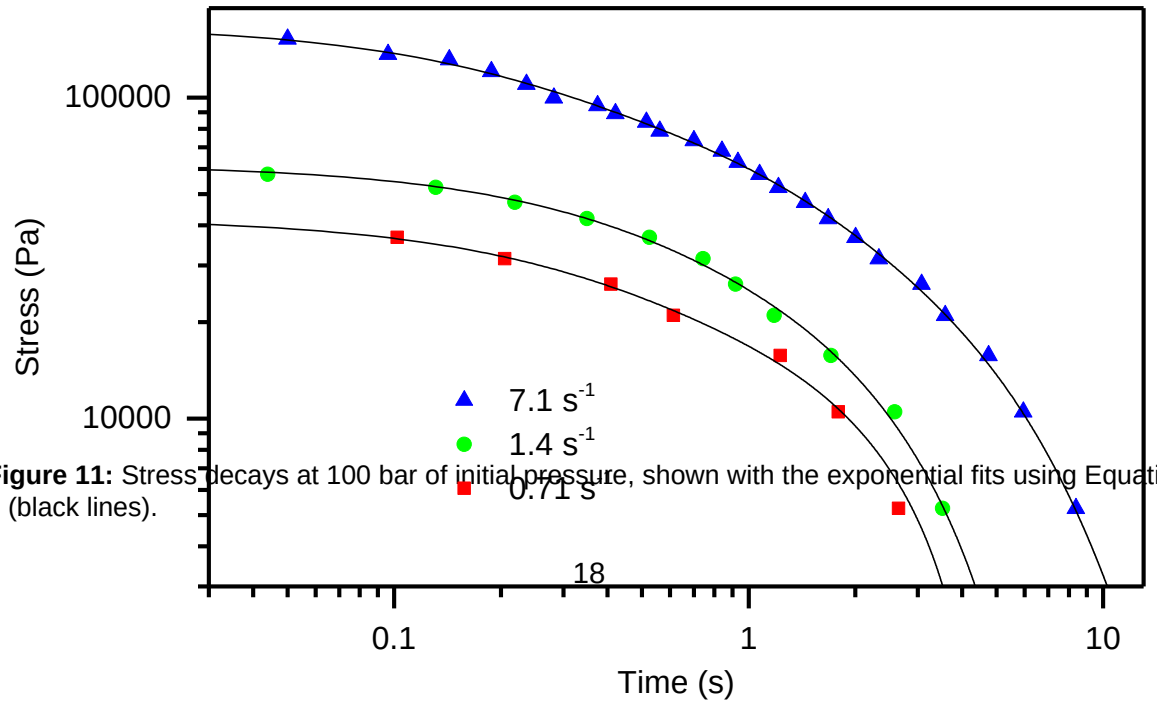

Figure 11: Stress decays at 100 bar of initial pressure, shown with the exponential fits using Equation 5 (black lines).

decay τ_1 was seen to be most significant at the highest speeds and pressures.

Relaxation times

The early and late relaxation times were found to be in line with the Rouse and reptation times respectively, determined from the linear rheology and scaling. Both early and late relaxation times were seen to increase with applied pressure (Figure 12). The relaxation times from both the pressure drop and stress fringes were compared and were seen to give similar values but the pressure drop results produced significantly more variation. No clear dependence of the relaxation time with shear rate was noted (Figure 13). Hence an average of the late relaxation time could be calculated across the different shear rates, which reduced the variation and still showed a positive relationship with pressure (Figure 14). To quantify this relationship, they were fitted with beta values according to the equations,

$$\beta_{\mathrm{E}} = \frac{d\ ln(\tau_1)}{d\ p} \tag{6}$$

$$\beta_{\mathrm{L}} = \frac{d\ ln(\tau_2)}{d\ p} \tag{7}$$

where β_E represents the pressure dependence of the early relaxation time τ_1 and β_L represents the pressure dependence of the late relaxation time τ_2.

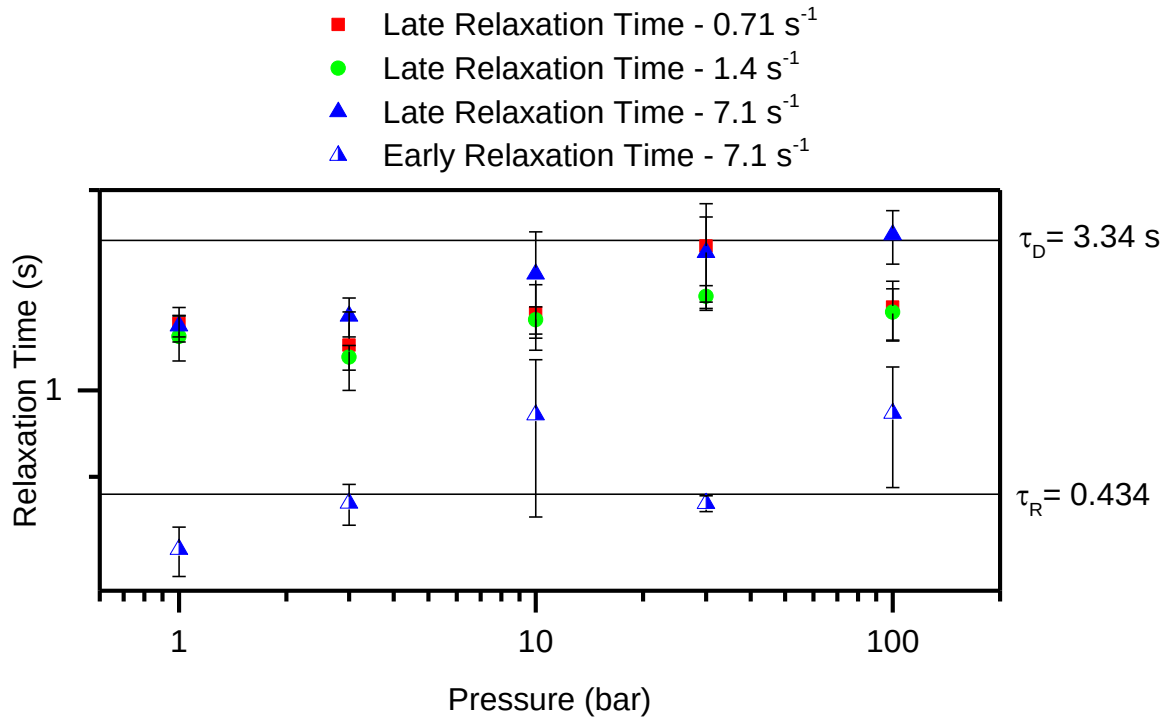

Figure 12: Early (τ_1) and late (τ_2) relaxation times extracted from exponential fits of the stress decays at different pressures using Equation 5. The Rouse and reptation times obtained from oscillatory rheology at 1 bar are annotated as horizontal lines for comparison.

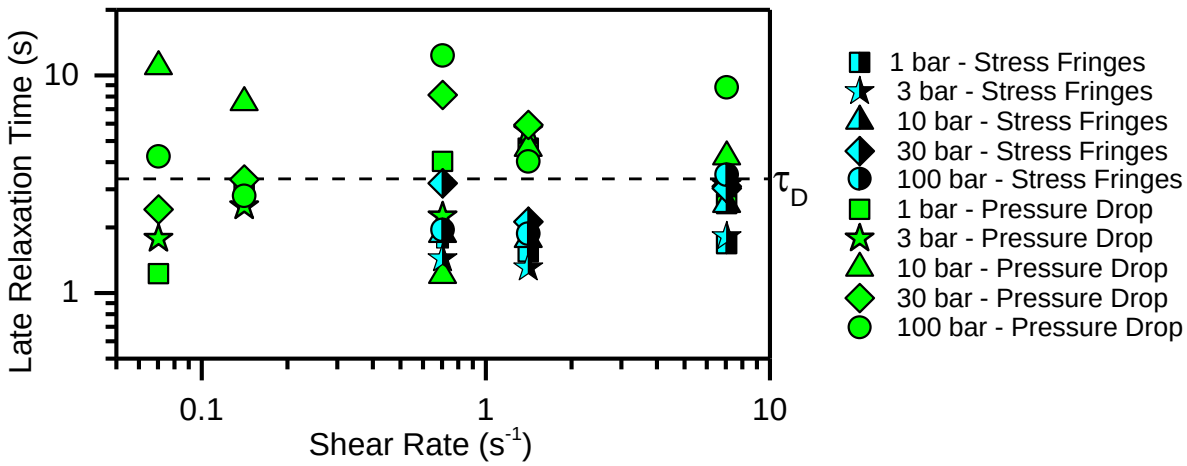

Figure 13: Late (reptation) relaxation times shown at different shear rates (proportional to piston speed, see Table I). Both those obtained from exponential fits of the stress and pressure drop decays are shown, the pressure referred to is the initial pressure applied before the shear. The reptation time obtained from oscillatory rheology at 1 bar (3.34 s) is annotated as a horizontal line for comparison.

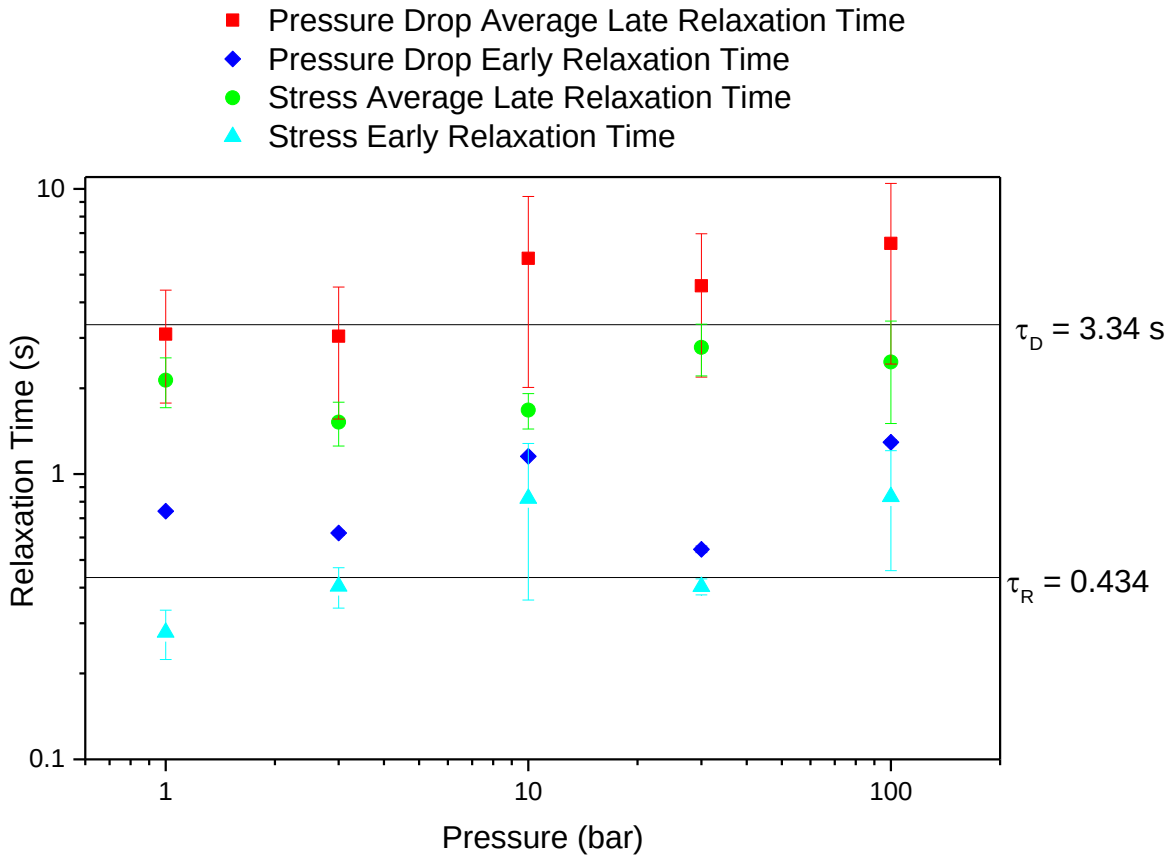

Figure 14: Early (Rouse) and late (reptation) relaxation times calculated from fits to both pressure drop and stress decays. The late relaxation times are averaged over all shear rates, whereas the Early relaxation time is only seen at the highest shear rate. The Rouse and reptation times obtained from oscillatory rheology at 1 bar are annotated as horizontal lines for comparison.

Discussion

Shear rheology

The fit to the data in Figure 3 captures the terminal crossover and rubbery region well, although slightly overestimates the complex moduli in the terminal region. In the GPC curve (supplementary material A), a small step can be seen at the lowest molecular weight, which could indicate some lower molecular weight chains were not detected. The presence of additional short chains could have contributed to the difference in the terminal region, although these also would be expected to have an effect on the plateau modulus. Nevertheless, the key features of the data for determination of characteristic relaxation times

of the polymer are well captured by this model which uses the measured molecular weight distribution data as input parameters.

The reptation time from the REPTATE [28] materials database is 9.24 s for 315k monodisperse linear PS at 170 °C. The inverse of the crossover of G'/G'' in the linear rheology differs significantly from this, giving a value of 3.34 s. The polydispersity of the sample, particularly the inclusion of shorter chains, causes this shift to a faster reptation time. The Rouse time is less dependent on the polydispersity and the value extracted from the fit to data (0.434 s) is similar to the expected value for monodisperse 315 K polystyrene (0.379 s from the REPTATE [28] materials database).

Multi-pass rheometry

Steady state stresses and pressures

The two lowest shear rates showed relatively little build-up of stress (1-1.5 fringes). At these piston speeds, the wall shear rates are below the inverse reptation time and so the polymers can fully relax on a shorter timescale than it takes to build up a deformation of order 1. On this basis, it might be considered surprising that any stress fringes at all are observed, since Wi_R is much less than one. However the calculated data in Table II shows there is a significant proportion of chains that are above their inverse reptation times at all piston speeds, and a small fraction may even fall into the $Wi_R > 1$ regime. The faster speeds showed significantly higher stress birefringence as an increasing proportion of the molecular weight distribution is unable to relax.

The extracted viscosities and β values are included here as a method of comparing results with existing literature and ensure consistency before discussing the more novel stress decays. Steady shear data from the rotational rheometer is provided alongside the complex viscosity extracted from the oscillatory measurements, to demonstrate that the Cox-Merz rule holds for this material. However, there is a relatively small region of overlap due to the

difficulty in obtaining results at high shear rates in the rotational rheometer without encountering slip and the sample escaping the gap.

The viscosities extracted from the fringe counting were significantly higher than for the pressure drop results at the same speed, and the values from fringe counts showed better agreement with the complex viscosity. This is due to the contribution of the entry and exit effects to the pressure drop which are minimised when counting fringes by only examining those in the gap. These additional contributions to the strain could have reduced the viscosity of the material (since it is a shear thinning polymer). The stress calculated from the pressure drop is therefore lower than that from fringe counting, which gives rise to the lower apparent viscosity.

It has been observed that β values vary when determined from different techniques (involving different methods of calculation) [17]. Comparing the β values obtained by stress fringes to those from pressure drop analysis in our experiments, however, there is some deviation between the two methods, but it is not systematic and differences are close to the range of error (Figure 9). The value of the SOC used could be a contributing factor as it is an average over many experiments and is seen to vary with shear rate (see supplementary material B for details). The uncertainty in the SOC of 0.2×10^{-9} Pa^{-1} is achieved by fitting to many measurements, whereas it is of the order 1×10^{-9} Pa^{-1}, (+/-20 %) in individual measurements. There is a much greater error in the values extracted from the pressure drop and the values fluctuate more significantly. This is likely due to effects outside the slit that cause fluctuations in viscosity, and could be reduced by recording more points at different pressures should a more accurate β be required from pressure drop alone. Since at the two lowest shear rates, a change in the number of fringes with pressure could not be separated from the error (0.5 fringes), effect measured by the change in pressure drop may not have been due to shear in the slit, and could have been dominated by exit and entry, which could have caused the anomalous results at these shear rates.

As the experiments were designed to span a logarithmic range of pressures (in order to study the stress relaxations) there is significant error introduced by fitting the limited range of points on a linear pressure scale. Despite this, it appears that values of β obtained with the MPR are in line with those obtained by other techniques. Notably, Kamal [8] obtained a value of 20.7 GPa^{-1} for PS at 2500 s^{-1} and Sedlacek *et al.* [7] obtained a shear independent (zero-shear) value of 43.45 ± 12.1 GPa^{-1}. Volpe *et al.* [37] reported values in the range 5-40 GPa^{-1}, for PS at temperatures in range 220-260 °C and showed the value decreased with shear rate. As discussed in the introduction, it can be difficult to obtain reliable values of the pressure coefficient as strictly it is defined only at a specific shear rate and temperature. For the values extracted from both the stress fringes and pressure drop, β is seen to increase with shear rate. This appears to contradict some reports in literature which show an increase [10, 15], or that suggest β is independent of shear rate Goubert *et al.* [38]. The β values are plotted against shear rate in supplementary material D.

Pressure drop decays

The pressure drop decays following cessation of flow were seen to follow a complex decay. This could however be modelled using several exponential decays (as in a simple Maxwell model of viscoelasticity [27]) with different timescales expected to be present in a polymer melt. There is expected to be relaxation due to both Rouse motion and reptation, which explains the presences of two different regimes, however there was also noted a third regime, very fast decay at very short times (much shorter than the Rouse time). This was seen at all pressures, although the magnitude of the decay occurring in this region increased with pressure and shear rate, making it most noticeable at the highest shear rates and pressures. This could be due to compressibility effects, which have been shown to affect the decays greatly at short times. For example, during a deformation we see pressure build up before the contraction in the geometry (causing the pressure drop across the geometry), which would cause some compression of the polymer before the geometry. On stopping the

pistons, the polymer could continue to flow to recover this change in density (as the volume between the pistons is kept constant), as well as relaxing stress *via* polymer motion.

Ranganathan *et al*. [18] observed for HDPE in an MPR, the presence of different regimes in the flow curve. As piston speed was increased, they observed a discontinuity in the pressure drop which suggested a region of unstable flow. Interestingly, the equivalent flow curves for polystyrene did not show any discontinuity, suggesting all our measurements were in the region of stable flow (Figure 15), and that flow instability cannot account for the different relaxation rates that are apparent in the stress and pressure drop decays. Ranganathan modelled pressure drop decay in this region using an adapted version of the Molenaar-Koopmans model for pressure changes during capillary flow, and showed that compressibility played an important part in the stress decay. Valette *et al.* [34] expanded on this by using Rolie-Poly [39] (based on viscoelasticity) and Carreau-Yasuda [40] (based on compressibility) models to calculate pressure drop decays for LLDPE, and showed that the decays were more dominated by compressibility effects early on and viscoelastic effects later in the decay, and the decay could be well represented using a Rolie-Poly model incorporating compressibility. We would expect our decays to be particularly dictated by the viscoelasticity of the polymer because of the broad plateau region measured in the linear rheology (and hence broad viscoelastic relaxation spectrum of the polymer). Hatzikiriakos and Dealy [41] note that short rise times to steady state (as seen in our experiments, on the scale of a few seconds) usually produce viscoelastically driven flows, and compressibility driven flows are usually characterised by rise times of several hours.

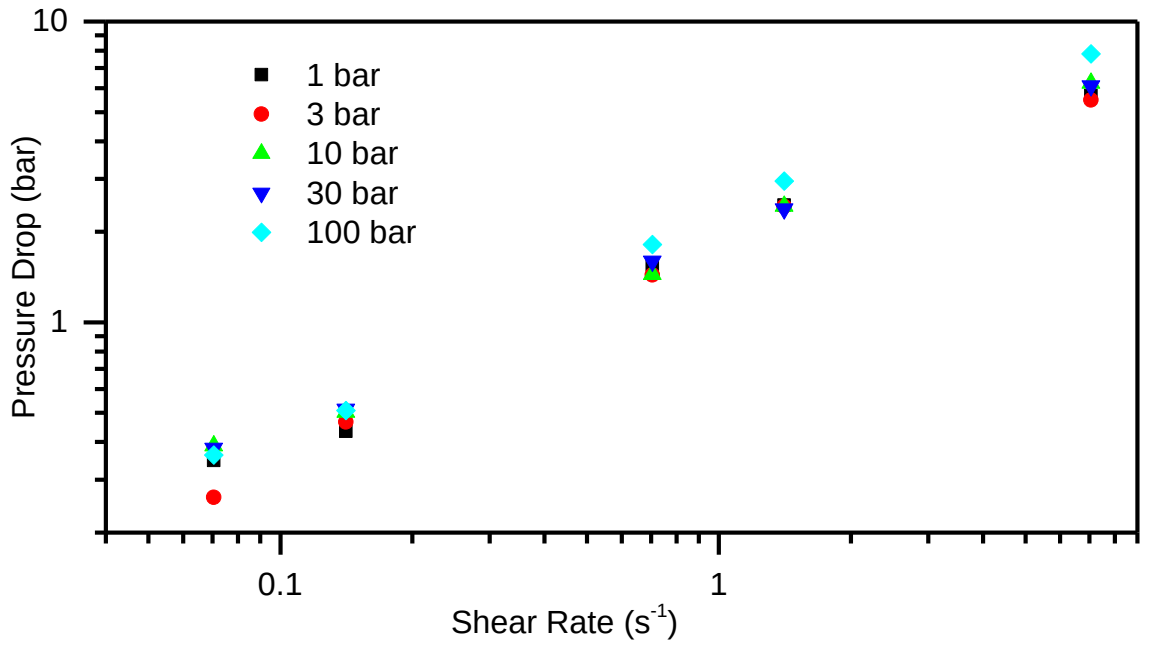

Figure 15: Flow curve of polystyrene at all pressures. The points show a power law relationship and show no discontinuity

It is therefore valid to assume that the decays seen are mostly dominated by viscoelasticity. However, since compressibility effects are seen at very short times it seems unlikely that the fast decay seen in our results is part of the polymer relaxation, and therefore can be separated out from the viscoelastic relaxation times.

It was initially postulated that the fast decay could be due to the polymer continuing to flow after the pistons have stopped. However, when the flow stop time was calculated (see supplementary material E) for this instrumental geometry, it was shown to be ~1.5 ms. This is a shorter time than the frame rate of the camera, hence could not have an effect on our results. It is also unlikely that the polymer leaking into some gap or part of the system that was not fully sealed, could contribute to the fast relaxation observed. Great care was taken to fully seal the cavity, and any such loss would cause the pressure and stress to decrease during the deformation, resulting in a decrease rather than a constant steady state.

However, a very small overshoot is noted in the retreating lower piston (for example 0.02 mm for a 15 mm stroke at 0.5 mm/s and 100 bar pressure). This overshoot is not present for the advancing top piston, and so would cause a small relaxation is pressure and stress.

Despite the small magnitude of this effect with respect to the stroke amplitude, it may have caused the initial fast decay of stress observed. Careful observation of particles present in the recorded videos supports this. Observing a single particle in the flow, a stop in motion is noted on stopping the pistons, after which a little forward flow continues (Figure 16). This suggests that there is an initial abrupt stop in movement, followed by the small overshoot in movement of the retreating piston causing the residual forwards flow (within 0.1 s of the stop in movement). This effect is likely the origin of the abnormally fast decays, which occur on a similar timescale (~0.1s).

Predictions from linear rheology suggest the mean Rouse time should only contribute at the highest shear rate, however it is was possible to observe the early relaxation time from experiments at 1.4 s^{-1} and 0.69 s^{-1}. This is consistent with our calculations from the GPC which suggest 5-10% chains are still above their inverse Rouse times at these rates.

At shear rates exceeding the inverse reptation time, the magnitude of the pressure drop is seen to increase with shear rate, and a significant increase is seen in the number of stress fringes. Nevertheless, a significant pressure drop is observed following flow cessation after the shear rates below the inverse reptation time, as well as stress fringes (1-1.5). The GPC analysis suggests this is due to the presence of higher molecular weight chains, as at all speeds there are significant amounts of chains (> 25%) above their inverse reptation time, and the longest relaxation times are predicted to dominate viscoelastic effects.

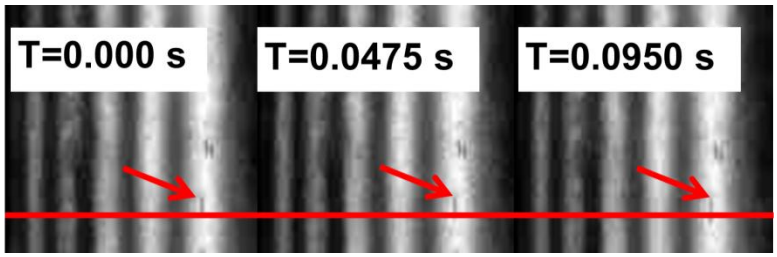

Figure 16: First three frames of video after piston stopped (noted from fringe decay) after a deformation at 0.1 mm/s at 10 bar initial pressure. A particle can be seen to stop between the first two frames before continuing to move a little, indicating residual flow due to overshoot of the lower piston.

Stress decays

Since the pressure drop across the geometry is proportional to the wall shear stress, the stress should also be expected to decay exponentially. This is seen in our results and as with the pressure drop decays, three regimes are observed. The three term exponential fits therefore gave very good agreement with the experiment data.

As for the pressure drop, all three of these regions are only observable at the highest shear rate. The initial fast term again is most apparent at the highest shear rates and pressures. However it was not captured in many of the stress decays, likely because of the reduced frequency of points. The camera frame rate of 18 fps gives a frame every 0.0475 s and as the fast decay occurs on a timescale of around 0.1 s, there may not have been enough data to isolate it for some decays.

Relaxation times

The β values for calculated for the relaxation times with pressure each show a small positive value, with the exception of the pressure drop early relaxation times, which has a β value close to the level of error (as shown in Figure 14). The pressure drop early relaxation times are expected to be the most effected by error since the pressure drop fluctuates more than the stress fringes and the early relaxation time has a lower value than the late (so is more effected by short timescale fluctuations). Both the early and late stress relaxation times show a similar increase with pressure, which implies that both the local stretching and long range orientational relaxation are retarded by increasing pressure. The increased pressure causes a slowing in molecular movement, resulting in an increase in viscosity (as seen frequently in literature, for example [19]). This effect reduces the speed of both Rouse and reptation processes.

Overall no significant effect on relaxation time with shear rate is noted, as shown in Figure 13. Although the shear rate can change relative contribution from each the regime of the

relaxation behaviour, it would not be expected to influence the Rouse or reptation relaxation times directly.

There is clearly more fluctuation in the relaxation times obtained from the pressure drop decays than the stress fringes, however, the two methods are in relatively good agreement and the early and late relaxation times are distinct from one another in each case. Overall, the optical capability clearly provides a more accurate measure of the relaxation time and provides other benefits such as being able to see the distribution of stress around the geometry, allowing analysis of exit and entry effects and the identification of wall-slip effects.

It is unclear why the pressure drop gives slightly higher values for the relaxation time than the optical analysis. The offset term, necessary to facilitate the exponential fits since the pressure drop did not decay to zero, could have contributed to this difference. Despite this, the trends are consistent between methods, and using either pressure or stress data has been shown to give reliable information on the relaxation times of the polymer. This suggests relaxation times could be obtained from the pressure decays alone, e.g. for an opaque sample. Furthermore, because the nature of the MPR allows multiple experiments, multiple decays could be recorded and averaged in order to minimise fluctuations.

Conclusion

Using a multi-pass rheometer for study of stress decay on cessation of a contraction-expansion flow, it has been possible to elucidate the pressure dependence of the viscoelasticity of polystyrene melts as well as several aspects of the underlying molecular rheology. Results for the pressure dependence of viscosity were broadly in line with those obtained using other methods on similar materials. The decay of stress could be described by a sum of up to three characteristic relaxation processes. The fastest process, most apparent after high shear rates and high pressures, is thought to arise from apparatus compliance in the form of an overshoot of the retreating piston. The remainder of the relaxation can be described by two characteristic time scales, which correspond well to the

Rouse and reptation times of the polymer. Interestingly the stress measured is significant even at inverse shear rates slower than the mean reptation relaxation time. We believe that this is because the dispersity in molecular weight gives rise to a small fraction of material with much longer relaxation times, and significant chain orientation and even stretch are possible at low shear rates. The method is non-destructive to the sample and repeatable. With careful recording and observation of the stress fringes, relaxation times for a polymer can be extracted.

Supplementary Material

See Supplementary Material for the gel permeation chromatogram of the polystyrene, details of the calculation of the stress optic coefficient, the fitting parameters for the exponential fits to the stress, the dependence of the pressure coefficient on shear rate, details of the calculation of the flow stop time and calculation of the pressure dependence of the relaxation times.

Acknowledgements

We gratefully acknowledge financial support from Michelin R&D (Material Performance and Processability). The authors would like to acknowledge Dr Ian Robinson (Visiting Industrial Fellow, Durham University) for initial inspiration for the work.

References

[1] Williams, M. L., Landel, R. F., and Ferry, J. D., ‘‘The Temperature Dependence of Relaxation Mechanisms in Amorphous Polymers and Other Glass-forming Liquids,’’ Journal of the American Chemical Society **77**, 3701-3707 (1955).

[2] Ferry, J. D., *Viscoelastic Properties of Polymers* (Wiley, 1980).

[3] Dealy, J. M., and Wang, J., *Melt rheology and its applications in the plastics industry* (Springer Science & Business Media, 2013).

[4] Barus, C., ‘‘Note on the Dependence of Viscosity on Pressure and Temperature,’’ Proceedings of the American Academy of Arts and Sciences **27**, 13-18 (1891).

[5] Miller, A. A., ‘‘Analysis of the melt viscosity and glass transition of polystyrene,’’ Journal of Polymer Science Part A-2: Polymer Physics **6**, 1161-1175 (1968).

[6] Utracki, L. A., and Sedlacek, T., ‘‘Free volume dependence of polymer viscosity,’’ Rheologica Acta **46**, 479-494 (2007).

[7] Sedlacek, T., Zatloukal, M., Filip, P., Boldizar, A., and Saha, P., ‘‘On the effect of pressure on the shear and elongational viscosities of polymer melts,’’ Polymer Engineering & Science **44**, 1328-1337 (2004).

[8] Kamal, M. R., and Nyun, H., ‘‘The Effect of Pressure on the Shear Viscosity of Polymer Melts,’’ Transactions of The Society of Rheology **17**, 271-285 (1973).

[9] Volpe, V., and Pantani, R., ‘‘Effect of pressure on viscosity at high shear rates by using an injection molding machine,’’ AIP Conference Proceedings **1695**, 020060 (2015).

[10] Sorrentino, A., and Pantani, R., ‘‘Pressure-dependent viscosity and free volume of atactic and syndiotactic polystyrene,’’ Rheologica Acta **48**, 467-478 (2009).

[11] Sorrentino, A., and Pantani, R., ‘‘Determination of the effect of pressure on viscosity of an isotactic polypropylene,’’ Polymer Bulletin **70**, 2005-2014 (2013).

[12] Kadijk, S. E., and Van Den Brule, B. H. A. A., ‘‘On the pressure dependency of the viscosity of molten polymers,’’ Polymer Engineering & Science **34**, 1535-1546 (1994).

[13] Akdeniz, G., Yahsi, U., and Tav, C., ‘‘Viscous behavior of PS, PP, and ABS in terms of temperature and pressure-dependent hole fraction,’’ Journal of Applied Polymer Science **117**, 110-113 (2010).

[14] Fernández, M., Muñoz, M. E., and Santamaría, A., ‘‘A Combined Analysis of PVT and Rheological Measurements: Novel Results for Three Amorphous Polymers,’’ Macromolecular Chemistry and Physics **209**, 1730-1737 (2008).

[15] Cardinaels, R., Van Puyvelde, P., and Moldenaers, P., ‘‘Evaluation and comparison of routes to obtain pressure coefficients from high-pressure capillary rheometry data,’’ Rheologica acta **46**, 495-505 (2007).

[16] Park, H. E., and Dealy, J. M., ‘‘Effects of Pressure and Supercritical Fluids on the Viscosity of Polyethylene,’’ Macromolecules **39**, 5438-5452 (2006).

[17] Park, H. E., Lim, S. T., Laun, H. M., and Dealy, J. M., ‘‘Measurement of pressure coefficient of melt viscosity: drag flow versus capillary flow,’’ Rheologica Acta **47**, 1023-1038 (2008).

[18] Ranganathan, M., Mackley, M., and Spitteler, P., ‘‘The application of the multipass rheometer to time-dependent capillary flow measurements of a polyethylene melt,’’ Journal of Rheology (1978-present) **43**, 443-451 (1999).

[19] Mackley, M. R., and Spitteler, P. H. J., ‘‘Experimental observations on the pressure-dependent polymer melt rheology of linear low density polyethylene, using a multi-pass rheometer,’’ Rheologica Acta **35**, 202-209 (1996).

[20] Aho, J., and Syrjälä, S., ‘‘Measurement of the pressure dependence of viscosity of polymer melts using a back pressure-regulated capillary rheometer,’’ Journal of Applied Polymer Science **117**, 1076-1084 (2010).

[21] Friesenbichler, W., Duretek, I., Rajganesh, J., and Kumar, S. R., ‘‘Measuring the pressure dependent viscosity at high shear rates using a new rheological injection mould,’’ Polimery **56**, 58-62 (2011).

[22] Housiadas, K. D., ‘‘Internal viscoelastic flows for fluids with exponential type pressure-dependent viscosity and relaxation time,’’ Journal of Rheology **59**, 769-791 (2015).

[23] Tsolou, G., Harmandaris, V. A., and Mavrantzas, V. G., ‘‘Molecular dynamics simulation of temperature and pressure effects on the intermediate length scale dynamics and zero shear rate viscosity of cis-1, 4-polybutadiene: Rouse mode analysis and dynamic structure factor spectra,’’ Journal of Non-Newtonian Fluid Mechanics **152**, 184-194 (2008).

[24] Floudas, G., Gravalides, C., Reisinger, T., and Wegner, G., ‘‘Effect of pressure on the segmental and chain dynamics of polyisoprene. Molecular weight dependence ’’ Journal of Chemical Physics **111**, 9847-9852 (1999).

[25] Mackley, M., Marshall, R., and Smeulders, J., ‘‘The multipass rheometer,’’ Journal of Rheology (1978-present) **39**, 1293-1309 (1995).

[26] Mackley, M. R., and Hassell, D. G., ‘‘The multipass rheometer a review,’’ Journal of Non-Newtonian Fluid Mechanics **166**, 421-456 (2011).

[27] Gargallo, L., and Radic, D., *Physicochemical Behavior and Supramolecular Organization of Polymers* (Springer, 2009).

[28] Ramirez, J., and Likhtman, A. E., ‘‘Rheology of Entangled Polymers: Toolbox for the Analysis of Theory and Experiments (Reptate, http://www.reptate.com),’’.

[29] Likhtman, A. E., and McLeish, T. C. B., ‘‘Quantitative Theory for Linear Dynamics of Linear Entangled Polymers,’’ Macromolecules **35**, 6332-6343 (2002).

[30] Viovy, J. L., Rubinstein, M., and Colby, R. H., ‘‘Constraint release in polymer melts: tube reorganization versus tube dilation,’’ Macromolecules **24**, 3587-3596 (1991).

[31] Des Cloizeaux, J., ‘‘Relaxation of entangled polymers in melts,’’ Macromolecules **23**, 3992-4006 (1990).

[32] Vorselaars, B., “Theory Documentation: Polydisperse Double Reptation.” *‘Rheology of Entangled Polymers: Toolbox for the Analysis of Theory and Experiments (Reptate, http://www.reptate.com)*.

[33] Van Ruymbeke, E., Liu, C.-Y., and Bailly, C., ‘‘Quantitative tube model predictions for the linear viscoelasticity of linear polymers,’’ (2007).

[34] Valette, R., Mackley, M. R., and del Castillo, G. H. F., ‘‘Matching time dependent pressure driven flows with a Rolie Poly numerical simulation,’’ Journal of non-newtonian fluid mechanics **136**, 118-125 (2006).

[35] Venerus, D., Zhu, S.-H., and Öttinger, H., ‘‘Stress and birefringence measurements during the uniaxial elongation of polystyrene melts,’’ Journal of Rheology (1978-present) **43**, 795-813 (1999).

[36] Coventry, K., “Cross-slot rheology of polymers,” University of Cambridge, (2006).

[37] Volpe, V., and Pantani, R., ‘‘Determination of the effect of pressure on viscosity at high shear rates by using an injection molding machine,’’ Journal of Applied Polymer Science, n/a-n/a (2017).

[38] Goubert, A., Vermant, J., Moldenaers, P., Göttfert, A., and Ernst, B., ‘‘Comparison of measurement techniques for evaluating the pressure dependence of the viscosity,’’ Applied Rheology **11**, 26-37 (2001).

[39] Likhtman, A. E., and Graham, R. S., ‘‘Simple constitutive equation for linear polymer melts derived from molecular theory: Rolie–Poly equation,’’ Journal of Non-Newtonian Fluid Mechanics **114**, 1-12 (2003).

[40] Yasuda, K., Armstrong, R. C., and Cohen, R. E., ‘‘Shear flow properties of concentrated solutions of linear and star branched polystyrenes,’’ Rheologica Acta **20**, 163-178 (1981).

[41] Hatzikiriakos, S. G., and Dealy, J. M., ‘‘Start-up pressure transients in a capillary rheometer,’’ Polymer Engineering & Science **34**, 493-499 (1994).